# Phase engineering of nanomaterials

Ye Chen[2†], Zhuangchai Lai[2†], Xiao Zhang[2†], Zhanxi Fan[1†], Qiyuan He[3†], Chaoliang Tan[2], and Hua Zhang[1,2*]

[1]Department of Chemistry, City University of Hong Kong, Tat Chee Avenue, Kowloon, Hong Kong, China

[2]Center for Programmable Materials, School of Materials Science and Engineering, Nanyang Technological University, Singapore 639798, Singapore

[3]Department of Materials Science and Engineering, City University of Hong Kong, Tat Chee Avenue, Kowloon, Hong Kong, China

†These authors contribute equally to this work.

*Correspondance to H.Z.
E-mail: hua.zhang@cityu.edu.hk

**Abstract**

Phase has emerged as an important structural parameter — in addition to composition, morphology, architecture, facet, size and dimensionality — that determines the properties and functionalities of nanomaterials. In particular, unconventional phases in nanomaterials that are unattainable in the bulk state can potentially endow nanomaterials with intriguing properties and innovative applications. Great progress has been made in the phase engineering of nanomaterials (PEN), including synthesis of nanomaterials with unconventional phases and phase transformation of nanomaterials. This Review provides an overview on the recent progress in PEN. We discuss various strategies used to synthesize nanomaterials with unconventional phases and induce phase transformation of nanomaterials, by taking noble metals and layered transition metal dichalcogenides as typical examples. Moreover, we also highlight recent advances in preparation of amorphous nanomaterials, amorphous–crystalline and crystal phase-based hetero-nanostructures. We also provide personal perspectives on challenges and opportunities in this emerging field, including exploration of phase-dependent properties and applications, rational design of phase-based heterostructures, and extension of the concept of phase engineering to a wider range of materials.

## [H1] Introduction

Nanomaterials can exhibit various crystalline and amorphous phases. If the crystal phases consist of ordered and periodic atomic arrangements, the amorphous ones are characterised by a disordered arrangement of the atoms. Although the prevailing phase of a material is primarily determined by the nature of its atomic bonding and thermodynamic parameters such as temperature and external pressure, many materials are found to possess more than one phase[1,2]. Conventionally, phase control has been achieved in some bulk materials using high pressure or thermal treatments[3]. For instance, under high pressure, many crystalline materials, such as ice[4] and α-quartz[5], can become amorphous and amorphous materials like metallic glass can become crystalline[6]. Importantly, phase changes often cause changes in the physicochemical properties of a material that can then find use in innovative applications. For example, materials, such as GeSbTe alloy can reversibly change their phase in response to stimuli like heat or laser irradiation, becoming promising for rewriteable data storage devices[7,8].

Phase engineering is more feasibly achieved in nanomaterials than in their bulk counterparts, because the growth of nanomaterials is determined by their surface characteristics, in addition to kinetics and thermodynamics[9,10]. Therefore, it is possible to tune various structural parameters of nanomaterials in a highly controllable manner by fine-tuning the experimental conditions. In many cases, the final structure of a nanomaterial is driven by the kinetic control of its synthetic process, in which a thermodynamically less favourable structure could be realized[11]. Such delicate control of the synthetic process of nanomaterials is of great importance to uncover the correlation between structure, property and application that benefits the rational design of nanomaterials. Furthermore, the discovery and manipulation of unconventional phases in

nanomaterials allow us to explore further their intriguing properties and a variety of promising applications, in addition to offering us new fundamental insights.

In past decades, many advances have been made in structure engineering of nanomaterials to achieve unique mechanical[12], electronic[13], optical[14], catalytic[15] and magnetic[16] properties. Distinct from the conventional strategies to engineer the composition, morphology, architecture, facet, size and dimensionality of nanomaterials, phase engineering provides another effective and powerful way to modulate their physicochemical properties and functions[17-19]. Specifically, phase engineering of nanomaterials (PENs) requires a deep understanding of the direct synthesis of nanomaterials with unconventional phases, phase transformation among conventional and unconventional phases of nanomaterials, growth of phase-based heterostructures, and preparation of amorphous and amorphous–crystalline heterophase nanomaterials.

In this Review, we first provide a brief introduction to PEN. Then we describe representative types of nanomaterials — specifically, noble metal and transition metal dichalcogenide (TMD) nanomaterials —with different conventional and unconventional phases. Thereafter, we discuss phase engineering strategies for these representative materials, including the direct synthesis and phase transformation, and briefly describe phase-dependent properties and applications. Subsequently, we introduce methods to prepare amorphous and amorphous–crystalline heterophase nanomaterials. Examples of crystal phase-based heterostructures and superstructures will also be highlighted. Finally, we discuss the major challenges and new opportunities in this emerging field of PEN.

## [H1] Conventional and unconventional phases in nanomaterials

Conventionally, a nano-sized material adopts the same phase as its bulk counterpart. However, unconventional phases that are not commonly observed in the bulk state have been

observed in different categories of nanomaterials, such as metals[20,21], metal oxides[22], two-dimensional (2D) layered compounds like TMDs[23] and group-IVA metal chalcogenides[19]. We use noble metals and TMDs as representative nanomaterials to illustrate the various strategies for PEN. Below we first introduce their different phases — conventional and unconventional ones — before delving in the phase engineering strategies.

The phases of metals nanomaterials, especially noble metal ones, are simple and composed of only non-directional metallic bonds. The hard-ball models in Fig. 1a illustrate the unit cells and characteristic packing sequences of the close-packed planes of different phases found in noble metal nanomaterials, namely face-centered cubic (*fcc*, or 3C), 2H and 4H-types of hexagonal close-packed (*hcp*) (*hcp*-2H type, *hcp*-4H type) crystal phases. Their close-packed planes, either *fcc* (111) or *hcp* (0001), are identical but packed in different sequences along the direction perpendicular to the close-packed planes. The characteristic packing sequences of *fcc*, 2H and 4H are identified as ABC, AB, and ABCB, respectively. The polymorphs that exhibit identical stacking layers but only differ by their stacking sequence are also known as polytypes[24]. In addition to crystalline phases, noble metal nanomaterials can also adopt amorphous phases, in which metal atoms are non-closely packed and in a random order.

As another typical group of polytypic materials, TMDs are layered compounds featuring intralayer covalent bonds and interlayer van der Waals (vdW) interactions. In general, layered TMDs crystalize into different phases based on the arrangement of the chalcogen and transition-metal atoms as well as the layer stacking sequence (Fig. 1b). For example, several different phases have been observed in the case of $MoS_2$, that mainly include the hexagonal (2H), octahedral (1T), rhombohedral (3R) and the distorted octahedral phase (1T'). 2H-$MoS_2$ and 3R-$MoS_2$ are polytypes with the same individual layer but different stacking sequences (Fig. 1b), whereas 1T and 1T' phases exhibit a different crystal structure symmetry from 2H

and 3R. The $1T_d$ phase, which is only observed in $MoTe_2$ and $WTe_2$, has the same single layer as 1T' phase but a different stacking sequence.

**[H1] Phase engineering of noble metal nanomaterials**

The structure–property relationship of noble metal nanomaterials has been substantially investigated in the past decades owing to their unique physicochemical properties and wide range of applications. As a newly emerged parameter, phase, especially unconventional ones, of noble metal nanomaterials can greatly affect properties and applications of these nanomaterials[20]. Current PEN strategies for noble metals include the direct synthesis of monometallic and multimetallic nanomaterials, and phase transformation between conventional and unconventional phases. Importantly, the PEN strategies may also be used to explore other non-noble metal or even non-metal nanomaterials for promising applications.

**[H2] Direct synthesis of noble metal nanomaterials with unconventional phases**

Wet-chemical syntheses have been used to directly prepare metal nanostructures with unconventional phases. Depending on the synthetic strategy, monometallic and multimetallic nanomaterials with single-phase or multiple-phase components can be obtained.

**[H3] Monometallic nanomaterials**. Generally, it is difficult to directly produce monometallic nanomaterials with phases other than their thermodynamically stable ones. Unconventional crystal phases in metals were early observed in sputtered metal films, such as 4H-Ag (REF.[25]) and 2H-Ni (REF.[26]). Theoretical studies suggest that the phase transition of nanosized metal is closely related to the environmental temperature and the particle size[27], both of which are critical factors affecting the free energy of metal nanostructures.. The size-dependent phase formation has been observed and theoretically studied for electrochemically deposited Ag nanowires[28]. Coexistence of 4H and *fcc* phases was observed for the obtained Ag nanowires, in which the 4H phase decreases with the increase of their diameter[28].

Although some experimental and theoretical results suggest that it is possible to obtain metal nanomaterials with unconventional phases, their direct and high-yield synthesis remains challenging. Colloidal synthetic methods that enable a control on the phase of noble metal nanostructures are particularly difficult to define because the phase of nanomaterials is ultimately affected by a number of parameters, such as combinations and concentrations of metal precursor, surface ligand, additive and solvent used during their synthesis. A typical phase-sensitive synthetic approach that involves the use of the $HAuCl_4$–oleylamine mixture has been reported to produce a variety of unconventional crystal phases of Au — including 4H (REF.[29]) (Fig. 2a) and 2H (REF.[30]) (Fig. 2b) phases as well as 2H/*fcc* (REF.[31]) and 4H/*fcc* (REF.[32]) (Fig. 2c) crystal-phase heterostructures. Interestingly, each of these unconventional phases was obtained by a slight change of synthesis conditions[33]. 4H nanoribbons are synthesized in the presence of dichloropropane, whereas the absence of dichloropropane and decrease of $HAuCl_4$–oleylamine ratio lead to the formation of Au nanorods with randomly alternated 4H and *fcc* phases. Similar 4H/*fcc* heterophases with low content of the 4H phase have also been observed in one-dimensional Ag nanostructures[34,35].

Ru precursor–polyol mixture has also been used to achieve control over the phase of nanomaterials. For example, *fcc* and *hcp* Ru nanoparticles can be obtained by using $RuCl_3$–ethylene glycol and Ru acetylacetonate–triethylene glycol, respectively[36].

**[H3] Multimetallic nanomaterials**. To further expand the library of crystal phases of metals and exploit unconventional phases toward enhanced performances in applications, one may consider nanomaterials containing more than one metal element, such as metal heterostructures or alloys. A commonly adopted strategy to prepare metal heterostructures with unconventional phases is the crystal phase-based template growth, in which a secondary metal epitaxially grows on the metal template (regardless of the original crystal phase of the secondary metal) to form either core–shell or branched structure[37-39]. For example, although

bulk Ru crystallizes in 2H phase, nanosized heterostucutres featuring 4H Ru (REF.[40]) or *fcc* Ru (REF.[41]) (Fig. 2d) have been obtained by using pre-synthesized 4H Au and *fcc* Pd nanostructures as templates, respectively. The unconventional phases of Ru could be preserved even after completely etching the templates, indicating their possible chemical stability[41,42].

More phase combinations can be attained for metal alloys because metals that are immiscible in bulk state can become miscible at nanoscale[43] and can lead to unconventional crystal phases, as in the case of some intermetallic compounds[44-47].

One effective strategy is to simultaneously reduce the precursors of the two metal structures that would crystalize in different phases in the bulk alloy. The resulting crystal phases can be tuned by controlling the composition of each metal precursor or reduction kinetics. For example, by controlling the reduction rate of Au and Ru precursors it was possible to control the crystal phases in $AuRu_3$ alloy nanoparticles (Fig. 2e)[43,48]. The resultant *fcc* and 2H $AuRu_3$ nanoparticles have identical composition and similar morphology, serving as ideal models for the study of the phase–property relation[49]. Furthermore, when the reduction rates of the two metal precursors vary at different growth stages, possibly due to the concentration change of the metal precursors and reducing agent, and/or the galvanic replacement reaction between one pre-reduced metal and the other metal ions in the growth solution, a complex structure with unconventional phase may be formed, in which the alloy composition and crystal phase are distributed differently throughout the structure[50,51]. For example, a crystal phase-based PtNi alloy hetero-nanostructure consisting of a Pt-rich *fcc* core and several Ni-rich 2H branches with Pt-rich edges has been synthesized (Fig. 2f)[50]. The strategies to fine-tune the composition, morphology and phase distribution of multicomponent metallic nanomaterials with unconventional phases provide more opportunities to modulate their properties toward desired applications.

## [H2] Phase transformation in noble metal nanomaterials

Phase transformation offers an alternative approach to the phase engineering of metal nanomaterials. Phase transformation leads to the formation of new nanostructures that might not be directly prepared using conventional synthetic methods. Different experimental approaches have been developed to achieve phase transformations of metal nanomaterials, including the use of surface modification[52], high pressure[53], high temperature[54] and electron beam irradiation[30].

**[H3] Surface modification.** As the size of materials decreases to the nanometre scale, their surface-to-volume ratio dramatically increases with the surface energy becoming the main contribution to the total system energy[55]. Therefore, the crystal phases of nanomaterials could be modulated by rationally tuning their surface energy[56,57]. Different surface modification methods, such as ligand exchange and metal coating as observed on the thin Au nanostructures, have been developed to realize the phase transformation of metal nanomaterials[52]. A complete phase transformation of Au square sheets (AuSSs) from 2H to *fcc* phases was observed by exchanging oleylamine with thiols on the surface of the nanostructures, leading to the formation of unique $(100)_f$-oriented AuSSs (Fig. 3a)[52]. Thiol molecules with different kinds of chemical structures can all induce the complete phase transformation of AuSSs, suggesting that the strong interaction between Au atom and –SH group might be the main driving force for the phase transformation. This is a new phase transition mechanism for close-packed metals as the close-packed directions of AuSSs changed after the phase transformation. It is worth mentioning that commonly, the close-packed directions are maintained in the phase transitions of close-packed metals. The ligand-exchange method can also be used to the phase transformation of Au nanoribbons from $(110)_{4H}$-oriented 4H to $(100)_f$-oriented *fcc* phases (Fig. 3a)[52].

Phase transformation of thin Au nanostructures induced by metal coating was found to be affected by many factors, such as ligand type, lattice mismatch between different metals and crystal phase stability[29,52,58]. It was observed that Ag coating on AuSSs achieved in the absence of oleylamine induced a complete phase transformation from $(110)_{2H}$-oriented 2H to $(100)_{f}$-oriented *fcc* phases (Fig. 3b)[52]. In contrast, in the presence of oleylamine, only a partial phase change of AuSSs from $(110)_{2H}$-oriented 2H to $(101)_{f}$-oriented *fcc* phases was observed. Pd and Pt coating on AuSSs in the absence of oleylamine induced not only a complete phase transformation from $(110)_{2H}$-oriented 2H to $(101)_{f}$-oriented *fcc* phases, but also a shape change of the AuSS from square to rhombic[58]. Coating of different metals on 4H Au nanoribbons in the absence of oleylamine can, instead, only induce a partial phase change from $(110)_{4H}$-oriented 4H to $(101)_{f}$-oriented *fcc* phases, enabling the stabilization of unconventional 4H phase in a series of metal nanostructures[29,38].

**[H3] High pressure.** As a fundamental thermodynamic parameter, pressure can induce the phase transformation of nanomaterials by directly altering the interatomic distances[59]. Importantly, by integrating diamond anvil cell and X-ray diffraction techniques, the crystal phase evolution of nanomaterials as a function of pressure can be in-situ monitored[59]. For example, a gradual phase transition of Pd nanocubes from highly symmetric *fcc* to low symmetric face-centered tetragonal (*fct*) could be observed by cold compressing the nanocubes from 0.3 GPa to 24.8 GPa[60]. Another study showed that *fcc* Ag nanoparticles of 5–10 nm undergo a reversible rhombohedral distortion under hydrostatic pressures up to 10 GPa (REF.[61]). In addition, a multistep phase transformation, from 2H to *fcc* at 1.03 GPa and then from *fcc* to *fct* at 12 GPa, was observed in Ag nanoplates under nonhydrostatic pressures[62]. Very recently, the phase transition of unconventional 4H-based Au nanostructures was investigated under high pressure (Fig. 3c). Unlike the common 2H-to-*fcc* phase transition in

metals, an irreversible phase transformation from 4H to *fcc* that involved the flattening of $(\bar{1}12)_{4H}$ planes was observed[53].

**[H3] High temperature.** The atomic rearrangement occurring under annealing at high temperature can change the crystal phase of nanomaterials[63]. High temperature treatments have been intensively used to induce the phase transformation of nanostructures with two or more metals, such as Pt-based and Pd-based nanocrystals[16,54,64-67]. Specifically, multi-metallic nanostructures with a chemically disordered phase (for example, *fcc*) are usually synthesized using a colloidal method. The obtained disordered nanostructures can be annealed at high temperature to obtain multi-metallic nanostructures with a chemically ordered phase (for example, *fct*). Such high temperature-induced phase transition could dramatically affect the physicochemical properties of the nanomaterial[63]. For instance, the phase transformation of FePt nanoparticles from *fcc* to *fct* achieved at temperature above 500 °C substantially increases the chemical stability of the nanoparticles and induces a change in their magnetic property, from paramagnetic to ferromagnetic[54,65]. The catalytic activity and stability of $Pt_3Co$ nanoparticles towards oxygen reduction can be substantially improved after the phase transformation from chemically disordered *fcc* to chemically ordered simple cubic (*sc*) at 700 °C (Fig. 3d)[54].

**[H3] Electron beam irradiation.** Compared to the aforementioned methods, electron beam irradiation, for example under a transmission electron microscope (TEM), has the advantage of enabling the direct observation of the phase transformation in nanomaterials with high spatial and temporal resolutions[68]. During TEM imaging, a portion of the electron energy dissipated from the incident electron beam and its interaction with the sample is converted in to heat[68]. Depending on the intensity and voltage of incident electron beam, the local temperature of the sample can reach even 500 °C (REF.[69]). For example, upon electron beam

irradiation for just a few minutes, the crystal phase of AuSSs completely transformed from 2H to *fcc*[30].

When two adhering noble metal nanostructures with different crystal phases are irradiated under the electron beam, size-dependent phase transformation from a thermodynamically stable phase to less stable unconventional phase can be observed. For instance, when a 7 nm Au nanoparticle with *fcc* phase adheres to the 4H nano-domain of an Au nanorod with diameter of 15 nm, the phase of the former can completely transform into 4H (Fig. 3e). However, such kind of phase transformation cannot be realized when the size of *fcc*-Au nanoparticle increases to 12 nm[70]. Besides the crystal phase transformation, electron beam irradiation can also initiate the crystallization of metal nanomaterials from their amorphous phase (for example, in the case of Bi nanoparticles[71]), providing another efficient way to uncover the nucleation and growth mechanism of nanomaterials.

**[H1]Phase engineering of transition metal dichalcogenide nanomaterials**

Crystal phase is one of the most important parameters of layered TMDs to determine their fascinating electronic, optical and chemical properties[17,72,73]. For instance, 2H-$MoS_2$ is semiconducting and intensively studied as one of the channel material for next-generation field emission transistors[74], whereas 1T-$MoS_2$ and 1T'-$MoS_2$, which are metallic and semi-metallic, respectively, are very promising non-precious metal catalysts for the electrocatalytic hydrogen evolution reaction (HER)[75,76]. The variety of phases in TMDs may be ascribed to the different electronic structures of their transition metal atoms, which depend on the different filling states of the *d* orbitals[17]. However, rational synthetic strategies to realize the phase-selective growth of TMDs remains limited. Although most of the highly stabile 2H-TMDs (such as 2H-$MoS_2$ and 2H-$WS_2$) and some 1T' TMDs (such as 1T'-$MoTe_2$ and 1T'-$WTe_2$) can be prepared using chemical vapor transport (CVT) and chemical vapor deposition (CVD), most of the metallic and semi-metallic TMDs, including 1T'-$MoS_2$ and 1T'-$WS_2$, still

remain difficult to synthesize because of their metastable nature[76-79]. Therefore, much effort has been devoted to the synthesis of metastable 1T or 1T' TMDs with high phase purity. Current synthetic strategies to engineer especially unconventional phases of TMDs can be categorized into two main types: direct phase-controlled synthesis and phase transformation of pre-synthesized, thermodynamically stable TMDs. Phase transformation can be achieved using various techniques, such as alkali metal ion intercalation[80-82], laser irradiation[76,83], plasmonic treatment[84] and electric field induced phase transition[85].

**[H2] Direct synthesis of transition metal dichalcogenides with unconventional phases**

The key to achieve the direct synthesis of metastable phase TMDs, such as 1T and 1T' phases, is to control the experimental conditions to facilitate the formation of metastable phases rather than conventional stable phases. A proper choice of precursors, especially those containing alkali metal ions, in gas–solid synthesis could be an effective way to obtain TMDs with unconventional phases[76,86]. For example, the first direct synthesis of metastable 1T-$MoS_2$ was realized by removing the potassium ions from $KMoS_2$ that was previously obtained by the reaction of $K_2MoO_4$ with $H_2S$, followed by 72-hour treatment with a mixture of $H_2$ and $N_2$ gas[86]. Metastable 1T'-$MoS_2$ and 1T'-$MoSe_2$ with high phase purity have also been produced using solid-state reaction and different precursors[76]. The precursors were prepared by reacting $K_2MoO_4$ with S or Se powder at 450 °C for 1.5 hours, followed by heating at 850 °C for 10 hours, all under $H_2$ and Ar gas flow. The precursors were then washed with deionized water and a solution of $I_2$ in acetonitrile to produce 1T'-$MoS_2$ and 1T'-$MoSe_2$. The as-prepared sub-centimetre 1T'-$MoS_2$ crystals (Fig. 4a) exhibit high phase purity and the characteristic distorted octahedral structure of the 1T' phase (Fig. 4b). More importantly, the mechanically exfoliated 1T'-$MoS_2$ nanosheet exhibited better performance than 2H-$MoS_2$ for the electrocatalytic HER, with an onset overpotential of 65 mV and a current density of 607 mA $cm^{-2}$ at 400 mV (versus reference hydrogen electrode)[76].

Liu and co-workers used $K_2MoS_4$ as precursor and proposed that $K^+$ can aid the growth of stable 1T'-$MoS_2$ monolayers using CVD (Fig. 4c)[78]. A proper choice of the substrate is also important for the successful growth of 1T'-$MoS_2$ (Fig. 4d). The use of mica as substrate leads to the growth of well-defined and uniform single-layer 1T'-$MoS_2$ nanosheets, with better results than those attained using substrates like $SiO_2$ and Si, highly ordered pyrolytic graphite, sapphire, NaCl crystals, quartz and Au foils[87]. This may be attributed to the ability of mica to trap $K^+$ ions from the precursor, owing toits unique structure and composition. Moreover, by using the CVD-grown single-layer TMD as a substrate, heterostructured TMDs such as the 1T'–2H $MoS_2$ bilayers can be fabricated[78]. This substrate-oriented phase-selective growth behaviour of TMDs may also be applied to the phase engineering of other materials with similar growth mechanism such as other TMDs with 1T' phase.

Direct solution-based synthesis, especially the commonly used colloidal synthesis, is another approach to realize TMDs with unconventional phases. The proper combination of reacting species often plays the key role in determining the phase of final product. For example, colloidal synthesis of 1T'-$WS_2$ is obtained by heating the mixture of $WCl_6$, $CS_2$, oleic acid and oleylamine at 320 °C, and 2H-$WS_2$ can be prepared by the addition of hexamethyldisilazane[77]. The strong coordinating interaction of the oleic acid — or other strong coordinating ligand such as dodecanethiol — and tungsten is found to be critical in the formation of the metastable 1T' phase[76]. In another report, the growth of branched few-layered 1T'-$WSe_2$ nanosheets is realized by the reaction of tungsten carbonyl ($W(CO)_6$), oleic acid, and Se in trioctylphosphine at 300 °C[79]. The high supersaturation of $WSe_2$ at the synthesis temperature is proposed to be the key to form the 1T' phase regardless of the types of tungsten and selenium precursors and the coordinating solvent. The prepared 1T'-$WSe_2$ nanosheets exhibit metallic properties and show higher electrocatalytic activity toward HER as compared to the annealed 2H counterpart. The crystal phase of $MoS_2$ synthesized using the

hydrothermal method has also been found to be temperature-dependent[88]. The reaction of $MnO_3$, thioacetamide and urea at 200 °C leads to the formation of metallic $MoS_2$, whereas the same reaction performed at 240 °C leads to semiconducting $MoS_2$. The pressurized hydrothermal environment with suitable reductant and temperature could be the key to the formation and stabilization of the metastable metallic $MoS_2$ intermediate, which may be used for the synthesis of other metastable TMDs.

**[H2] Phase transformation in transition metal dichalcogenides.** Metastable phases of TMDs can also be produced by transformation of thermodynamically stable phases. Depending on the phase transition technique used, the metastable phases can appear either in localized domains or in more extended areas of the final product. Understanding the phase transformation behaviour of TMDs is of fundamental importance to further extend their practical applications in electronics and catalysis[17,72,73,89]. Phase transition strategies of TMDs from thermodynamically stable phases to metastable phases can be divided into two categories: direct electron injection and thermal activation. The former mainly involves the charge transfer process from external sources to the transition metal atoms; the latter results from the absorption of external energy such as high-energy phonons and electrons.

**[H3] Direct electron injection.** Direct electron injection can be achieved through chemical and electrochemical intercalation, and electrostatic doping.

Chemical intercalation of alkyl metal ions is the most commonly used method to induce phase transition in TMDs and obtain their metastable phases (Fig. 4e). This approach dates back to 1980s, when $MoS_2$ was exfoliated into monolayers using Li intercalation[90]. The most studied case is Li intercalation of $MoS_2$ using *n*-butyllithium, in which the coordination of Mo changed from trigonal to octahedral as a result of the charge injection from the alkyl lithium to the *d*-orbitals of the Mo atoms[91-93]. Two octahedral metastable phases were

typically observed in the transition process: 1T phase without distortion and 1T' phase with distorted zig-zag Mo chains. However, by performing the *n*-butyllithium treatment on microsized TMD crystals, only 1T phase was observed in ultrasmall TMD nanodots, indicating that the size of TMDs could also affect the crystal phase[80]. These metastable phases can easily be identified using Raman, photoluminescence, X-ray photoelectron spectroscopy (XPS) and X-ray diffraction (XRD), but the detailed structure of the metallic 1T and semi-metallic 1T' phases can only be distinguished using scanning TEM (STEM). Quantitative information on the mixed phases is usually estimated based on the deconvolution of high-resolution XPS peaks.

Compared to the chemical intercalation**,** the electrochemical approach[82,94] offers higher efficiency, the possibility to use diverse intercalants and a better control over the intercalation kinetics. This method uses the electrochemical potential in an electrochemical cell to drive the intercalants into the vdW gaps of TMDs. Metal ions such as $Li^+$, $Na^+$, $K^+$, $Mg^{2+}$, as well as alkylammonium cations[95,96] can be electrochemically intercalated into the layer gaps of TMDs (Fig. 4e), inducing their partial phase transition from 2H to 1T or 1T'. The electrochemical platform is compatible with various techniques for in-situ characterization to resolve the evolution of structural, electrical, optical and optoelectronic properties during the intercalation process[97,98].

Hot electron injection from plasmonic nanoparticles[84], interfacial charge diffusion from 2D electride[99] and direct electron-beam irradiation[100] are other charge transfer processes that can induce phase transition in TMDs. Unlike chemical and electrochemical intercalation, which can produce metastable phases over extended areas, these methods induce localized phase transition within the direct-contact regions.

Field-induced phase transition in TMDs was proposed in a theoretical study of TMD monolayers exposed to a high-magnitude electrical field using thin dielectric[101]. This approach was later realized using exceptionally strong electrostatic doping in ionic gating (Fig. 4f) owing to the electrical-double-layer capacitor formed at the TMD–electrolyte interface[85] (Fig. 4g). In electrostatic doping, electrons are injected into the conduction band of the 2H phase, which has significantly lower energy than that of the 1T' phase. When the doping concentration is high enough to achieve a total energy for the 2H phase higher than the total energy of 1T' phase, the structure of TMD changes and the phase transitions from 2H to 1T'. Gating in ionic liquid can produce an ultra-strong field in the range of 10 MV $m^{-1}$ with a doping concentration ($n_{2D}$) exceeding $10^{14}$ $cm^{-2}$, making such phase transition feasible. Experimentally, the fully reversible phase transition of monolayer $MoTe_2$ occurs at an ionic gating voltage of ~ 3.0 V (REF.[85]), corresponding to the doping concentration of ~$0.85\times10^{14}$ when the kinetic barrier is excluded, which is in agreement with the theoretical prediction[101].

**[H3] Thermal activation.** Thermal activation covers strategies such as thermal annealing and laser irradiation.

Thermal annealing is an efficient way to restore the thermodynamically stable phase from the metastable phase, such as the phase transformation from 1T or 1T' to 2H in $MoS_2$ and $MoSe_2$ under elevated temperature[76]. In contrast, 1T'-$MoTe_2$ can be obtained by annealing 2H phase at an elevated temperature (above 500 ºC), as evident in the in-situ XRD and Raman characterizations[102]. The 1T' phase changes back to 2H phase upon slow cooling, indicating a reversible phase transition between 1T'- and 2H-$MoTe_2$.

Laser irradiation induces phase transition between stable and metastable phases through a local heating effect. Low power laser irradiation often restores a stable phase from a metastable one[76], while high power laser can also induce the formation of metastable phases

in some TMDs[83,103]. In $MoTe_2$, the local phase transition from 2H to 1T' is believed to be triggered by the formation of Te vacancy at an elevated temperature under strong laser irradiation[83]. Although very convenient, laser irradiation is often accompanied by a thinning effect[76,83] that removes the layers of the TMD crystals (Fig. 4h) and only the phase of top layer of the multi-layer $MoTe_2$ crystal can be effectively changed from 2H to 1T'[83]

Besides the aforementioned techniques, phase transition of TMDs can be achieved with a variety of external treatments such as those using mechanical force[104,105], plasma[106], supercritical $CO_2$ (REF.[107]) and covalent functionalization with organic molecules[108]. For example, tensile strain applied by an atomic force microscope (AFM) tip can significantly lower the phase transition temperature in $MoTe_2$ (REF.[104]). A small tensile strain of 0.2% at room temperature can successfully induce local phase transitions in $MoTe_2$ from 2H to 1T' that can be identified by the increase of conductivity in conductive AFM measurement[104]. Alternatively, transition from semiconducting to metallic phase occurs in $MoS_2$ in a diamond anvil cell when the pressure reaches ~ 19GPa, that likely arises from the sulphur–sulphur interactions between the layers when the vdW gap closes at high pressures[105]. In another example, high energy Ar plasma induces the local phase transition from 2H to 1T on a $MoS_2$ monolayer and creates mosaic structures with 1T domains of a few nanometres[106].

**[H2] Applications of phase transition in TMDs.** One of the most important results of phase transitions in TMDs is the conversion of their electronic band structures from semiconducting to semi-metallic or metallic. Phase engineering of TMD catalysts can significantly improve their electrocatalytic performance, due to a combination of much improved charge transport property and the higher intrinsic electrocatalytic activity of the metallic phase compared to the semiconducting one[76]. Moreover, by using phase-patterning technique based on chemical intercalation[81] or laser irradiation[83], the obtained metallic or semi-metallic phase TMD can be covered by metal electrodes to achievethe Ohmic contact in field effect transistors. The

Ohimic contact  is generally difficult to acieve owing to the strong Fermi-level pinning effect of TMD semiconductor with the common metal contact.

**[H1] Amorphous and amorphous–crystalline phases in nanomaterials.**

Controlled synthesis of inorganic nanomaterials with low degree of crystallinity — as in the case of amorphous phases or amorphous–crystalline heterophase — is of fundamental importance to engineer phases beyond ordered atomic arrangements. Amorphous materials exhibit random atomic arrangement or short-range order over just a few atoms that result in distorted lattices and/or dangling bonds (Fig. 5a). Conventional amorphous bulk materials, such as metallic glass and metal oxides, have attracted considerable interests because of their promising mechanical, catalytic and magnetic applications[109-111]. Recently, amorphous nanomaterials have emerged as a new category of functional nanomaterials with fascinating applications in catalysis[112,113], electronic devices[114] and lithium-ion batteries[115,116]. However, because of the high entropy resulted from the irregular atomic arrangement and unsaturated bonds, most amorphous materials are metastable and easily convertible into their crystalline state under external heat or pressure[117,118]. To date, synthesis of amorphous nanostructures has only been achieved in limited types of nanomaterials[119,120], such as metal or metal–metalloid alloys[121-123], metal oxides and hydroxides[124-126]. Here we discuss some proposed strategies to prepare nanomaterials with amorphous phase or amorphous–crystalline heterophase.

**[H2] Amorphous metal nanomaterials.** Amorphous metal nanomaterials are often obtained by capturing and maintaining the liquid-like intermediate state during the crystallization process of an ultrasmall or ultrathin metal nanocrystal. Such ‘frozen’ amorphous phases can be maintained by anchoring the material on a confining substrate[127,128], doping[121], and by using weak reducing agents[129,130] during the colloidal synthesis.

For instance, the presence of $CeO_x$ on a $CeO_x$–reduced graphite oxide bi-substrate is found to induce the amorphization of small Au nanoparticles[128]. Compared to the use of a bi-substrate, doping metals with small atoms like B and P, through the addition of reducing agents to the colloidal synthesis[121] or electroless deposition[131], is a more general strategy to prepare various amorphous metal alloys that involves the formation of amorphous metal boride or metal phosphide, as in the case of Pt-based and Pd-based amorphous alloys[132,133]. Crystallinity and electrical properties of these alloys can be tuned by changing the metal–metalloid composition[122]. Although in-depth studies on the structural characteristics of amorphous metal–metalloid alloy nanomaterials are still lacking, they have been demonstrated to be excellent catalysts for a wide range of catalytic reactions owing to their high density of unsaturated catalytic sites[134,135].

Although it is generally difficult to obtain completely amorphous phases without the addition of dopants or a substrate, metastable amorphous/crystalline heterophase can be easily formed, as observed in the colloidal synthesis of amorphous/crystalline Pd nanosheets with tunable crystallinity (Fig. 5b)[130]. The amount of crystalline domains in the Pd nanosheet increases with elevated reaction temperature. Interestingly, it is found that higher percentage of amorphous phase in the Pd nanosheets leads to a better chemoselectivity for the catalysis of 4-nitrostyrene hydrogenation, whereas higher percentage of crystalline phase results in a higher catalytic activity[130]. This temperature-sensitive nature of amorphous Pd nanosheets can also be exploited to prepare Pd alloy with different crystallinity[136].

**[H2] Amorphous semiconductor nanomaterials.** Besides metal-based amorphous nanomaterials, recently, various types of semiconductor-based amorphous nanomaterials have also attracted considerable interests[137,138]. Likewise, the amorphous nanostructures of semiconductors are prone to crystallization and require the addition of chemical stabilizers during the synthetic process. Early solution-phase preparations of amorphous materials were

usually performed using low-temperature (less than 400 ºC) metathetical reaction (such as, $TX_4+2A_2Y \rightarrow TY_2+4AX$, where *T* is the transition metal, *X* is salt anion, *A* is the alkali-like cation and *Y* is the chalcogenide anion)[139]. More recently, wet-chemical methods have been further developed for the preparation of amorphous metal sulfides, especially for amorphous $MoS_x$ nanostructures[140,141]. Diverse kinds of amorphous $MoS_x$, such as doped amorphous molybdenum sulfide[142] and $MoS_x$ clusters, such as $[Mo_3S_4]^{4+}$(REF.[143]), $[Mo_3S_7]$-thiolate[144], $[Mo_3S_{13}]^{2-}$(REF.[145]), or $[Mo_2S_{12}]^{2-}$(REF.[146]), have also been successfully prepared. The unique structures and scalable methods for the preparation of these amorphous materials make them promising and active catalysts for HER[147]. The outstanding catalytic performance of amorphous $MoS_x$ for HER appears to be related to its dynamic surface, that is, its continuous structural and chemical transformations during the electrochemical HER process[140]. Nonetheless, the initially active amorphous $MoS_x$ is found to gradually crystallize, resulting in its deactivation but higher turn-over frequency and better stability in HER[148].

Films of amorphous $MoS_x$ can be obtained by electrodeposition[149,150]. Usually, the Mo:S ratio for these $MoS_x$ films is lower than 1:2, which results in a large number of unsaturated S bonds and active sites for hydrogen production. Tran and co-workers prepared amorphous $MoS_x$ by electrochemical deposition of $[MoS_4](NH_4)_2$ onto fluorine-doped tin oxide substrate in phosphate buffer[147]. This amorphous $MoS_x$ shows a molecular-based coordination polymer structure consisting of $[Mo_3S_{13}]^{2-}$ building blocks (Fig. 5c)[147]. In another work, Ting and co-workers prepared amorphous $MoS_x$ on glassy carbon electrode by anodic or cathodic deposition from an aqueous electrolyte consisting of $(NH_4)_2[MoS_4]$ in 0.1 M KCl[150]. The bridging $S_2^{2-}$ rather than apical $S^{2-}$ in the amorphous $MoS_x$ shows high electron binding energies and serves as the active site for HER[150].

**[H2] Amorphization from crystalline materials.** Amorphous structures can also be obtained through the conversion of crystalline materials using external forces, such as

electricity[151], pressure[152] and lithiation[153]. This approach also enables one to effectively control the degree of crystallinity of a material. The electricity-induced amorphization process has been widely observed in phase-change materials that can reversibly switch between crystalline and amorphous state exhibiting different electronic and optical behaviours[151]. These kinds of materials, such as $Sb_2Te_3$, $Ge_1Sb_4Te_7$ and GeTe, have been widely investigated and applied as excellent non-volatile storage devices[151,154,155]. Compared to the electricity-induced amorphization, pressure-induced amorphization is a more general and powerful approach to induce atomic disorder in a wide range of nanomaterials[152,156,157]. Unlike the conventional amorphization process for bulk materials, the pressure-induced amorphization of nanomaterials is determined not only by the external pressure, but also by the characteristics of the nanomaterials, such as size and surface property[59]. Lithium treatment has emerged as another promising top-down approach to tune the structural characteristics of materials, especially for layered materials[82,158], as shown in the structural transformation of layered palladium phosphosulfide ($Pd_3P_2S_8$) crystal to amorphous lithium-incorporated palladium phosphosulfide nanodots (Fig. 5d). During the lithiation-induced amorphization process, several structural changes simultaneously occur that include decrease of dimension, size and crystallinity, vacancy formation and lithium incorporation[153]. Interestingly, the amorphization of layered $Pd_3P_2S_8$ crystals activates this inert material to become an efficient electrocatalytic catalyst for HER[153].

**[H1] Perspectives**

Although considerable progress has been made in phase engineering of nanomaterials (PENs), various challenges still need to be faced. Although different unconventional phases of nanomaterials have been discovered, studies on their phase-dependent properties and/or applications are rarely reported. An unneglectable question that comes with the discovery of an unconventional phase in nanomaterials concerns their stability. This can be evaluated

under different circumstances, such as elevated temperature and/or pressure, applied electric or magnetic fields, or certain atmospheres, during synthesis, storage, as well as under various conditions relevant to their applications. Although the metastable nature of unconventional phases may lead to interesting physicochemical properties, countermeasures to stabilize the as-prepared unconventional phases are required to enable further applications. It is worth mentioning that the synthetic and phase transformation strategies discussed in this Review may readily serve as guidelines for stabilization of nanomaterials with unconventional phases. Meanwhile, it remains challenging to simultaneously control the phase and morphology of nanomaterials. For example, it is still difficult to synthesize nanostructures with same or even similar morphologies but different phases for the study of their phase-dependent properties and applications, in which the effect of other structural characteristics could be excluded.

Despite the aforementioned challenges, there are many intriguing directions to be explored in PENs. For example, strategies involving electrochemistry or the use of electric field, magnetic field and optical irradiation could also be explored to induce the phase transformation of nanomaterials. It is highly desired to realize well-controlled phase transformation that is reversible or can be realized under mild conditions.

Defect engineering is another aspect of PENs that has attracted increasing interests for its great potentials to enhance the performances of nanomaterials in various applications. However, synthesis and stabilization of nanomaterials with ordered defects — that can be considered as a type of new phase — remains challenging. From the application-point-of-view, nanomaterials with particular structural characteristics and compositions are often desired to meet specific practical requirements, which calls for the rational design and preparation of heterophase nanostructures and their related hybrids, in which synergistic effects between different phases and/or different components could lead to enhanced performances in specific applications. Particularly, it would be intriguing to realize the well-

defined ordering of different phases in the crystal-phase-heterostructured or heterophased nanomamaterials[159].

The concepts and methodologies of PENs can be further developed in many other aspects. For example, phase engineering can be combined with other structure engineering strategies, such as composition, architecture or dimensionality engineering, to enable a higher level of control over various nanomaterials.

The development of phase engineering greatly relies on the advancement in characterization techniques for new phases in nanomaterials, especially the amorphous ones. Crystallographic information, including lattice parameters and degree of crystallinity, of nanomaterials can be characterized using advanced techniques, such as spherical aberration-corrected STEM, selected-area electron diffraction, XRD. The local atomic environment, such as bond length, coordination number and binding energy, can be revealed by XPS and X-ray absorption spectroscopy that are especially important in determining the amorphous phase in nanostructures. It can be foreseen that the future developments of characterization approaches that include various in-situ observation techniques will enable a deeper understanding of the formation and transformation mechanisms of different phases in nanomaterials.

Exploration and development of theoretical principles to guide the synthesis, stabilization and transformation of unconventional phases in nanomaterials are critically important for the establishment of theory-guided PENs. A current challenge lies in the lack of theoretical insights on the formation and transformation mechanisms of the unconventional phases in nanomaterials. One of the main reasons could be the difficulty of modelling atomic arrangements in unconventional phases, especially for the amorphous ones. The complicated and irregular atomic arrangement in amorphous nanomaterials makes it exceedingly difficult to build up convincing models or simulate their behaviours. Screening and prediction of new

phases, which have not been experimentally observed, could become possible with the aid of advanced high-performance computing systems or even artificial intelligence.

Last but not the least, the concept of PENs can also be applied to many other intensively explored materials with unique physicochemical properties and promising applications, such as metal–organic frameworks, covalent organic frameworks and perovskites. Down to the even smaller scale, strategies in PEN can be used to guide the synthesis and stabilization of single atoms, atom pairs, or other forms of atomic arrangements such as clusters. From a macroscopic point of view, phase engineering can also be employed to produce materials from building blocks beyond atoms and ions, including supercrystalline materials assembled from nanoclusters, nanoparticles or microparticles. Extending the concept of phase engineering to other kinds of materials opens up an avenue to discover novel functional materials for various promising applications.

**Acknowledgement**

This work was supported by MOE under AcRF Tier 2 (MOE2016-T2-2-103; MOE2017-T2-1-162) and AcRF Tier 1 (2017-T1-001-150; 2017-T1-002-119), NTU under Start-Up Grant (M4081296.070.500000), and Agency for Science, Technology and Research (A*STAR) under its AME IRG (Project No. A1783c0009) in Singapore. H.Z. thanks the support from ITC via Hong Kong Branch of National Precious Metals Material Engineering Research Center. Z.F., Q.H. and H.Z. thank the support from the Start-Up Grant in City University of Hong Kong.

**Author contributions**

All authors researched data for the article and contributed to the drafting and editing of manuscript.

**Competing interests**

The authors declare no competing interests.

## Publisher's note

## References


1 Porter, D. A., Easterling, K. E. & Sherif, M. *Phase Transformations in Metals and Alloys*. (CRC Press LLC, 2009).

2 William. D. Callister, D. G. R. *Materials Science and Engineering*. Eighth edn, 44-83 (John Wiley & Sons (Asia) Pte Ltd., 2011).

3 Sharma, S. M. & Sikka, S. K. Pressure induced amorphization of materials. *Prog. Mater. Sci.* **40**, 1-77 (1996).

4 Hemley, R. J., Chen, L. C. & Mao, H. K. New transformations between crystalline and amorphous ice. *Nature* **338**, 638-640 (1989).

5 Hemley, R. J., Jephcoat, A. P., Mao, H. K., Ming, L. C. & Manghnani, M. H. Pressure-induced amorphization of crystalline silica. *Nature* **334**, 52-54 (1988).

6 Zeng, Q. *et al.* Long-range topological order in metallic glass. *Science* **332**, 1404-1406 (2011).

7 Wuttig, M. & Yamada, N. Phase-change materials for rewriteable data storage. *Nat. Mater.* **6**, 824-832 (2007).

8 Hosseini, P., Wright, C. D. & Bhaskaran, H. An optoelectronic framework enabled by low-dimensional phase-change films. *Nature* **511**, 206-211 (2014).

9 Xia, Y., Xia, X. & Peng, H.-C. Shape-controlled synthesis of colloidal metal nanocrystals: thermodynamic versus kinetic products. *J. Am. Chem. Soc.* **137**, 7947-7966 (2015).

10 Klimov, V. I. *Semiconductor and Metal Nanocrystals: Synthesis and Electronic and Optical Properties*. (CRC Press, 2003).

11 Hollingsworth, J. A., Poojary, D. M., Clearfield, A. & Buhro, W. E. Catalyzed growth of a metastable InS crystal structure as colloidal crystals. *J. Am. Chem. Soc.* **122**, 3562-3563 (2000).

12 Wu, G., Chan, K. C., Zhu, L., Sun, L. & Lu, J. Dual-phase nanostructuring as a route to high-strength magnesium alloys. *Nature* **545**, 80-83 (2017).

13 Gong, Y. *et al.* Spatially controlled doping of two-dimensional $SnS_2$ through intercalation for electronics. *Nat. Nanotechnol.* **13**, 294-299 (2018).

14 Lu, A.-Y. *et al.* Janus monolayers of transition metal dichalcogenides. *Nat. Nanotechnol.* **12**, 744-749 (2017).

15 Asadi, M. *et al.* Nanostructured transition metal dichalcogenide electrocatalysts for $CO_2$ reduction in ionic liquid. *Science* **353**, 467-470 (2016).

16 Sun, S., Murray, C. B., Weller, D., Folks, L. & Moser, A. Monodisperse FePt nanoparticles and ferromagnetic FePt nanocrystal superlattices. *Science* **287**, 1989-1992 (2000).

17 Voiry, D., Mohite, A. & Chhowalla, M. Phase engineering of transition metal dichalcogenides. *Chem. Soc. Rev.* **44**, 2702-2712 (2015).

18 Li, H. & Wang, X. Phase control in inorganic nanocrystals through finely tuned growth at an ultrathin scale. *Acc. Chem. Res.* **52**, 780-790 (2019).

19 Wang, J., Wei, Y., Li, H., Huang, X. & Zhang, H. Crystal phase control in two-dimensional materials. *Sci. China Chem.* **61**, 1227-1242 (2018).

20 Fan, Z. & Zhang, H. Crystal phase-controlled synthesis, properties and applications of noble metal nanomaterials. *Chem. Soc. Rev.* **45**, 63-82 (2016).

21 Cheng, H., Yang, N., Lu, Q., Zhang, Z. & Zhang, H. Syntheses and properties of metal nanomaterials with novel crystal phases. *Adv. Mater.* **30**, 1707189 (2018).

22 Sood, S. & Gouma, P. Polymorphism in nanocrystalline binary metal oxides. *Nanomaterials and Energy* **2**, 82-96 (2013).

23 Wang, R. *et al.* Strategies on phase control in transition metal dichalcogenides. *Adv. Funct. Mater.* **28**, 1802473 (2018).
24 C Giacovazzo *et al. Fundamentals of Crystallography*. (Oxford University Press, 2011).
25 Taneja, P., Banerjee, R., Ayyub, P. & Dey, G. K. Observation of a hexagonal (4H) phase in nanocrystalline silver. *Phys. Rev. B* **64**, 033405 (2001).
26 Thomson, G. P. The crystal structure of nickel films. *Nature* **123**, 912 (1929).
27 Doye, J. P. & Calvo, F. Entropic effects on the size dependence of cluster structure. *Phys. Rev. Lett.* **86**, 3570-3573 (2001).
28 Liu, X., Luo, J. & Zhu, J. Size effect on the crystal structure of silver nanowires. *Nano Lett.* **6**, 408-412 (2006).
29 Fan, Z. *et al.* Stabilization of 4H hexagonal phase in gold nanoribbons. *Nat. Commun.* **6**, 7684 (2015).
30 Huang, X. *et al.* Synthesis of hexagonal close-packed gold nanostructures. *Nat. Commun.* **2**, 292 (2011).
31 Huang, X. *et al.* Graphene oxide-templated synthesis of ultrathin or tadpole-shaped Au nanowires with alternating hcp and fcc domains. *Adv. Mater.* **24**, 979-983 (2012).
32 Chen, Y. *et al.* High-yield synthesis of crystal-phase-heterostructured 4H/fcc Au@Pd core-shell nanorods for electrocatalytic ethanol oxidation. *Adv. Mater.* **29**, 1701331 (2017).
33 Fan, Z., Huang, X., Chen, Y., Huang, W. & Zhang, H. Facile synthesis of gold nanomaterials with unusual crystal structures. *Nat. Protoc.* **12**, 2367-2378 (2017).
34 Liang, H., Yang, H., Wang, W., Li, J. & Xu, H. High-yield uniform synthesis and microstructure-determination of rice-shaped silver nanocrystals. *J. Am. Chem. Soc.* **131**, 6068-6069 (2009).
35 Shen, X. *et al.* Anisotropic growth of one-dimensional silver rod-needle and plate-belt heteronanostructures induced by twins and hcp phase. *J. Am. Chem. Soc.* **131**, 10812-10813 (2009).
36 Kusada, K. *et al.* Discovery of face-centered-cubic ruthenium nanoparticles: facile size-controlled synthesis using the chemical reduction method. *J. Am. Chem. Soc.* **135**, 5493-5496 (2013).
37 Fan, Z. & Zhang, H. Template synthesis of noble metal nanocrystals with unusual crystal structures and their catalytic applications. *Acc. Chem. Res.* **49**, 2841-2850 (2016).
38 Fan, Z. *et al.* Epitaxial growth of unusual 4H hexagonal Ir, Rh, Os, Ru and Cu nanostructures on 4H Au nanoribbons. *Chem. Sci.* **8**, 795-799 (2017).
39 Fan, Z. *et al.* Synthesis of 4H/fcc noble multimetallic nanoribbons for electrocatalytic hydrogen evolution reaction. *J. Am. Chem. Soc.* **138**, 1414-1419 (2016).
40 Lu, Q. *et al.* Crystal phase-based epitaxial growth of hybrid noble metal nanostructures on 4H/fcc Au nanowires. *Nat. Chem.* **10**, 456-461 (2018).
41 Ye, H. *et al.* Ru nanoframes with an *fcc* structure and enhanced catalytic properties. *Nano Lett.* **16**, 2812-2817 (2016).
42 Lu, Q. *et al.* Synthesis of hierarchical 4H/fcc Ru nanotubes for highly efficient hydrogen evolution in alkaline media. *Small* **14**, 1801090 (2018).
43 Kobayashi, H., Kusada, K. & Kitagawa, H. Creation of novel solid-solution alloy nanoparticles on the basis of density-of-states engineering by interelement fusion. *Acc. Chem. Res.* **48**, 1551-1559 (2015).
44 Kusada, K. & Kitagawa, H. A route for phase control in metal nanoparticles: A potential strategy to create advanced materials. *Adv. Mater.* **28**, 1129-1142 (2016).

45 Vasquez, Y., Luo, Z. & Schaak, R. E. Low-temperature solution synthesis of the non-equilibrium ordered intermetallic compounds $Au_3Fe$, $Au_3Co$, and $Au_3Ni$ as nanocrystals. *J. Am. Chem. Soc.* **130**, 11866-11867 (2008).
46 Li, J. & Sun, S. Intermetallic nanoparticles: synthetic control and their enhanced electrocatalysis. *Acc. Chem. Res.* **52**, 2015-2025 (2019).
47 Yun, Q. *et al.* Synthesis of PdM (M = Zn, Cd, ZnCd) nanosheets with an unconventional face-centered tetragonal phase as highly efficient electrocatalysts for ethanol oxidation. *ACS Nano* **13**, 14329-14336 (2019).
48 Zhang, Q. *et al.* Selective control of fcc and hcp crystal structures in Au-Ru solid-solution alloy nanoparticles. *Nat. Commun.* **9**, 510 (2018).
49 Zhang, Q. *et al.* Crystal structure-dependent thermal stability and catalytic performance of $AuRu_3$ solid-solution alloy nanoparticles. *Chem. Lett.* **47**, 559-561 (2018).
50 Cao, Z. *et al.* Platinum-nickel alloy excavated nano-multipods with hexagonal close-packed structure and superior activity towards hydrogen evolution reaction. *Nat. Commun.* **8**, 15131 (2017).
51 Zhang, Z. *et al.* Crystal phase and architecture engineering of lotus-thalamus-shaped Pt-Ni anisotropic superstructures for highly efficient electrochemical hydrogen evolution. *Adv. Mater.* **30**, 1801741 (2018).
52 Fan, Z. *et al.* Surface modification-induced phase transformation of hexagonal close-packed gold square sheets. *Nat. Commun.* **6**, 6571 (2015).
53 Li, Q. *et al.* Pressure-induced phase engineering of gold nanostructures. *J. Am. Chem. Soc.* **140**, 15783-15790 (2018).
54 Wang, D. *et al.* Structurally ordered intermetallic platinum-cobalt core-shell nanoparticles with enhanced activity and stability as oxygen reduction electrocatalysts. *Nat. Mater.* **12**, 81-87 (2013).
55 Benaissa, H. & Ferhat, M. Polytypism-induced stabilization of hexagonal 2H, 4H and 6H phases of gold. *Superlattices Microstruct.* **109**, 170-175 (2017).
56 McHale, J. M., Auroux, A., Perrotta, A. J. & Navrotsky, A. Surface energies and thermodynamic phase stability in nanocrystalline aluminas. *Science* **277**, 788-791 (1997).
57 Zhang, H., Gilbert, B., Huang, F. & Banfield, J. F. Water-driven structure transformation in nanoparticles at room temperature. *Nature* **424**, 1025-1029 (2003).
58 Fan, Z. *et al.* Synthesis of ultrathin fcc Au@Pt and Au@Pd core-shell nanoplates from hcp Au square sheets. *Angew. Chem. Int. Ed.* **54**, 5672-5676 (2015).
59 Bai, F., Bian, K., Huang, X., Wang, Z. & Fan, H. Pressure induced nanoparticle phase behavior, property, and applications. *Chem. Rev.* **119**, 7673-7717 (2019).
60 Guo, Q. *et al.* Cubic to tetragonal phase transformation in cold-compressed Pd nanocubes. *Nano Lett.* **8**, 972-975 (2008).
61 Koski, K. *et al.* Structural distortions in 5–10 nm silver nanoparticles under high pressure. *Phys. Rev. B* **78**, 165410 (2008).
62 Sun, Y., Yang, W., Ren, Y., Wang, L. & Lei, C. Multiple-step phase transformation in silver nanoplates under high pressure. *Small* **7**, 606-611 (2011).
63 Liang, J. *et al.* Atomic arrangement engineering of metallic nanocrystals for energy-conversion electrocatalysis. *Joule* **3**, 956-991 (2019).
64 Alloyeau, D. *et al.* Size and shape effects on the order-disorder phase transition in CoPt nanoparticles. *Nat. Mater.* **8**, 940-946 (2009).
65 Kim, J., Lee, Y. & Sun, S. Structurally ordered FePt nanoparticles and their enhanced catalysis for oxygen reduction reaction. *J. Am. Chem. Soc.* **132**, 4996-4997 (2010).

66 Cui, Z., Li, L., Manthiram, A. & Goodenough, J. B. Enhanced cycling stability of hybrid Li–air batteries enabled by ordered $Pd_3Fe$ intermetallic electrocatalyst. *J. Am. Chem. Soc.* **137**, 7278-7281 (2015).
67 Qiu, Y. *et al.* BCC-phased PdCu alloy as a highly active electrocatalyst for hydrogen oxidation in alkaline electrolytes. *J. Am. Chem. Soc.* **140**, 16580-16588 (2018).
68 Zheng, H. *et al.* Observation of transient structural-transformation dynamics in a $Cu_2S$ nanorod. *Science* **333**, 206-209 (2011).
69 Smith, D. J., Petford-Long, A. K., Wallenberg, L. R. & Bovin, J.-O. Dynamic atomic-level rearrangements in small gold particles. *Science* **233**, 872-875 (1986).
70 Saleem, F. *et al.* Size-dependent phase transformation of noble metal nanomaterials. *Small* **15**, 1903253 (2019).
71 Li, J. *et al.* In situ atomic-scale study of particle-mediated nucleation and growth in amorphous bismuth to nanocrystal phase transformation. *Adv. Sci.* **5**, 1700992 (2018).
72 Tan, C. *et al.* Recent advances in ultrathin two-dimensional nanomaterials. *Chem. Rev.* **117**, 6225-6331 (2017).
73 Zhang, X., Lai, Z., Ma, Q. & Zhang, H. Novel structured transition metal dichalcogenide nanosheets. *Chem. Soc. Rev.* **47**, 3301-3338 (2018).
74 Radisavljevic, B., Radenovic, A., Brivio, J., Giacometti, V. & Kis, A. Single-layer $MoS_2$ transistors. *Nat. Nanotechnol.* **6**, 147-150 (2011).
75 Voiry, D. *et al.* Conducting $MoS_2$ nanosheets as catalysts for hydrogen evolution reaction. *Nano Lett.* **13**, 6222-6227 (2013).
76 Yu, Y. *et al.* High phase-purity 1T'-$MoS_2$- and 1T'-$MoSe_2$-layered crystals. *Nat. Chem.* **10**, 638-643 (2018).
77 Mahler, B., Hoepfner, V., Liao, K. & Ozin, G. A. Colloidal synthesis of 1T-$WS_2$ and 2H-$WS_2$ nanosheets: applications for photocatalytic hydrogen evolution. *J. Am. Chem. Soc.* **136**, 14121-14127 (2014).
78 Liu, L. *et al.* Phase-selective synthesis of 1T' $MoS_2$ monolayers and heterophase bilayers. *Nat. Mater.* **17**, 1108-1114 (2018).
79 Sokolikova, M. S., Sherrell, P. C., Palczynski, P., Bemmer, V. L. & Mattevi, C. Direct solution-phase synthesis of 1T' $WSe_2$ nanosheets. *Nat. Commun.* **10**, 712 (2019).
80 Tan, C. *et al.* Preparation of high-percentage 1T-phase transition metal dichalcogenide nanodots for electrochemical hydrogen rvolution. *Adv. Mater.* **30**, 1705509 (2018).
81 Kappera, R. *et al.* Phase-engineered low-resistance contacts for ultrathin $MoS_2$ transistors. *Nat. Mater.* **13**, 1128-1134 (2014).
82 Zeng, Z. *et al.* Single-layer semiconducting nanosheets: high-yield preparation and device fabrication. *Angew. Chem. Int. Ed.* **50**, 11093-11097 (2011).
83 Cho, S. *et al.* Phase patterning for ohmic homojunction contact in $MoTe_2$. *Science* **349**, 625-628 (2015).
84 Kang, Y. *et al.* Plasmonic hot electron induced structural phase transition in a $MoS_2$ monolayer. *Adv. Mater.* **26**, 6467-6471 (2014).
85 Wang, Y. *et al.* Structural phase transition in monolayer $MoTe_2$ driven by electrostatic doping. *Nature* **550**, 487-491 (2017).
86 Wypych, F. & Schollhorn, R. 1T-$MoS_2$, a new metallic modification of molybdenum disulfide. *J. Chem. Soc., Chem. Commun.*, 1386-1388 (1992).
87 Bampoulis, P., Sotthewes, K., Siekman, M. H., Zandvliet, H. J. W. & Poelsema, B. Graphene visualizes the ion distribution on air-cleaved mica. *Sci. Rep.* **7**, 43451 (2017).

88 Geng, X. *et al.* Pure and stable metallic phase molybdenum disulfide nanosheets for hydrogen evolution reaction. *Nat. Commun.* **7**, 10672 (2016).
89 Yang, H., Kim, S. W., Chhowalla, M. & Lee, Y. H. Structural and quantum-state phase transitions in van der Waals layered materials. *Nat. Phys.* **13**, 931-937 (2017).
90 Py, M. A. & Haering, R. R. Structural destabilization induced by lithium intercalation in $MoS_2$ and related compounds. *Can. J. Phys.* **61**, 76-84 (1983).
91 Eda, G. *et al.* Photoluminescence from chemically exfoliated $MoS_2$. *Nano Lett.* **11**, 5111-5116 (2011).
92 Sun, X., Wang, Z., Li, Z. & Fu, Y. Q. Origin of structural transformation in mono- and bi-layered molybdenum disulfide. *Sci. Rep.* **6**, 26666 (2016).
93 Sun, L. *et al.* Layer-dependent chemically induced phase transition of two-dimensional $MoS_2$. *Nano Lett.* **18**, 3435-3440 (2018).
94 Zeng, Z. *et al.* An effective method for the fabrication of few-layer-thick inorganic nanosheets. *Angew. Chem. Int. Ed.* **51**, 9052-9056 (2012).
95 Wan, C. *et al.* Flexible n-type thermoelectric materials by organic intercalation of layered transition metal dichalcogenide $TiS_2$. *Nat. Mater.* **14**, 622-627 (2015).
96 Wang, C. *et al.* Monolayer atomic crystal molecular superlattices. *Nature* **555**, 231-236 (2018).
97 Xiong, F. *et al.* Li Intercalation in $MoS_2$: in situ observation of its dynamics and tuning optical and electrical properties. *Nano Lett.* **15**, 6777-6784 (2015).
98 He, Q. *et al.* In situ probing molecular intercalation in two-dimensional layered semiconductors. *Nano Lett.* **19**, 6819-6826 (2019).
99 Kim, S. *et al.* Long-range lattice engineering of $MoTe_2$ by a 2D electride. *Nano Lett.* **17**, 3363-3368 (2017).
100 Lin, Y.-C., Dumcenco, D. O., Huang, Y.-S. & Suenaga, K. Atomic mechanism of the semiconducting-to-metallic phase transition in single-layered $MoS_2$. *Nat. Nanotechnol.* **9**, 391-396 (2014).
101 Li, Y., Duerloo, K.-A. N., Wauson, K. & Reed, E. J. Structural semiconductor-to-semimetal phase transition in two-dimensional materials induced by electrostatic gating. *Nat. Commun.* **7**, 10671 (2016).
102 Keum, D. H. *et al.* Bandgap opening in few-layered monoclinic $MoTe_2$. *Nat. Phys.* **11**, 482-486 (2015).
103 Guo, Y. *et al.* Probing the dynamics of the metallic-to-semiconducting structural phase transformation in $MoS_2$ crystals. *Nano Lett.* **15**, 5081-5088 (2015).
104 Song, S. *et al.* Room temperature semiconductor–metal transition of $MoTe_2$ thin films engineered by strain. *Nano Lett.* **16**, 188-193 (2016).
105 Nayak, A. P. *et al.* Pressure-induced semiconducting to metallic transition in multilayered molybdenum disulphide. *Nat. Commun.* **5**, 3731 (2014).
106 Zhu, J. *et al.* Argon plasma induced phase transition in monolayer $MoS_2$. *J. Am. Chem. Soc.* **139**, 10216-10219 (2017).
107 Qi, Y. *et al.* $CO_2$-induced phase engineering: protocol for enhanced photoelectrocatalytic performance of 2D $MoS_2$ nanosheets. *ACS Nano* **10**, 2903-2909 (2016).
108 Voiry, D. *et al.* Covalent functionalization of monolayered transition metal dichalcogenides by phase engineering. *Nat. Chem.* **7**, 45-49 (2014).
109 Smith, R. D. L. *et al.* Photochemical route for accessing amorphous metal oxide materials for water oxidation catalysis. *Science* **340**, 60-63 (2013).
110 Liu, Y. H. *et al.* Super plastic bulk metallic glasses at room temperature. *Science* **315**, 1385-1388 (2007).

111 Luo, Q., Zhao, D. Q., Pan, M. X. & Wang, W. H. Magnetocaloric effect in Gd-based bulk metallic glasses. *Appl. Phys. Lett.* **89**, 081914 (2006).
112 Morales-Guio, C. G. & Hu, X. Amorphous molybdenum sulfides as hydrogen evolution catalysts. *Acc. Chem. Res.* **47**, 2671-2681 (2014).
113 Anantharaj, S. & Noda, S. Amorphous catalysts and electrochemical water splitting: an untold story of harmony. *Small*, 1905779 (2019).
114 Liu, J. *et al.* All-amorphous-oxide transparent, flexible thin-film transistors. efficacy of bilayer gate dielectrics. *J. Am. Chem. Soc.* **132**, 11934-11942 (2010).
115 Wang, X. *et al.* Amorphous hierarchical porous GeOx as high-capacity anodes for Li ion batteries with very long cycling life. *J. Am. Chem. Soc.* **133**, 20692-20695 (2011).
116 Hall, J. W. *et al.* Low-temperature synthesis of amorphous $FeP_2$ and Its use as anodes for Li ion batteries. *J. Am. Chem. Soc.* **134**, 5532-5535 (2012).
117 Lu, K. Nanocrystalline metals crystallized from amorphous solids: nanocrystallization, structure, and properties. *Mater. Sci. Eng. R Rep.* **16**, 161-221 (1996).
118 Zhao, H., Chen, X., Wang, G., Qiu, Y. & Guo, L. Two-dimensional amorphous nanomaterials: synthesis and applications. *2D Materials* **6**, 032002 (2019).
119 Amstad, E. *et al.* Production of amorphous nanoparticles by supersonic spray-drying with a microfluidic nebulator. *Science* **349**, 956-960 (2015).
120 Nai, J., Kang, J. & Guo, L. Tailoring the shape of amorphous nanomaterials: recent developments and applications. *Sci. Chi. Mater.* **58**, 44-59 (2015).
121 Zhu, Z. *et al.* Facile synthesis of Co–B amorphous alloy in uniform spherical nanoparticles with enhanced catalytic properties. *ACS Catal.* **2**, 2119-2125 (2012).
122 Pei, Y. *et al.* Synthesis and catalysis of chemically reduced metal–metalloid amorphous alloys. *Chem. Soc. Rev.* **41**, 8140-8162 (2012).
123 Cheng, H. *et al.* Ligand exchange-induced amorphization of Pd nanomaterials for highly efficient electrocatalytic hydrogen evolution reaction. *Adv. Mater.*, 1902964 (2020).
124 Yan, S. *et al.* Research advances of amorphous metal oxides in electrochemical energy storage and conversion. *Small* **15**, 1804371 (2019).
125 Li, H. B. *et al.* Amorphous nickel hydroxide nanospheres with ultrahigh capacitance and energy density as electrochemical pseudocapacitor materials. *Nat. Commun.* **4**, 1894 (2013).
126 Indra, A. *et al.* Unification of catalytic water oxidation and oxygen reduction reactions: amorphous beat crystalline cobalt iron oxides. *J. Am. Chem. Soc.* **136**, 17530-17536 (2014).
127 Shi, M.-M. *et al.* Anchoring PdCu amorphous nanocluster on graphene for electrochemical reduction of $N_2$ to $NH_3$ under ambient conditions in aqueous solution. *Adv. Energy Mater.* **8**, 1800124 (2018).
128 Li, S. J. *et al.* Amorphizing of Au nanoparticles by CeOx -RGO hybrid support towards highly efficient electrocatalyst for $N_2$ reduction under ambient conditions. *Adv. Mater.* **29**, 1700001 (2017).
129 Duan, Y. X. *et al.* Amorphizing of Cu nanoparticles toward highly efficient and robust electrocatalyst for $CO_2$ reduction to liquid fuels with high Faradaic efficiencies. *Adv. Mater.* **30**, e1706194 (2018).
130 Yang, N. *et al.* Amorphous/crystalline hetero-phase Pd nanosheets: one-pot synthesis and highly selective hydrogenation reaction. *Adv. Mater.* **30**, e1803234 (2018).
131 Poon, K. C. *et al.* Newly developed stepwise electroless deposition enables a remarkably facile synthesis of highly active and stable amorphous Pd nanoparticle electrocatalysts for oxygen reduction reaction. *J. Am. Chem. Soc.* **136**, 5217-5220 (2014).

132 Ma, Y., Wang, R., Wang, H., Linkov, V. & Ji, S. Evolution of nanoscale amorphous, crystalline and phase-segregated PtNiP nanoparticles and their electrocatalytic effect on methanol oxidation reaction. *Phys. Chem. Chem. Phys.* **16**, 3593-3602 (2014).
133 Huang, H., Wang, H., Hu, W., Lv, W. & Ye, W. Exploring the role of nickel in the formation of amorphous Pt-based metallic alloys for methanol electro-oxidation with significant enhancement. *Electrochem. Commun.* **82**, 107-111 (2017).
134 He, D. *et al.* Amorphous nickel boride membrane on a platinum–nickel alloy surface for enhanced oxygen reduction reaction. *Nat. Commun.* **7**, 12362 (2016).
135 Nsanzimana, J. M. V. *et al.* An efficient and earth-abundant oxygen-evolving electrocatalyst based on amorphous metal borides. *Adv. Energy Mater.* **8**, 1701475 (2018).
136 Cheng, H. *et al.* Aging amorphous/crystalline heterophase PdCu nanosheets for catalytic reactions. *Natl. Sci. Rev.*, 955-961 (2019).
137 Bellus, M. Z., Yang, Z., Hao, J., Ping Lau, S. & Zhao, H. Amorphous two-dimensional black phosphorus with exceptional photocarrier transport properties. *2D Materials* **4**, 025063 (2017).
138 Morigaki, K. & Ogihara, C. *Amorphous semiconductors: structure, optical, and electrical properties*. (2017).
139 Chianelli, R. R. Amorphous and poorly crystalline transition metal chalcogenides. *Int. Rev. Phys. Chem.* **2**, 127-165 (1982).
140 Lee, S. C. *et al.* Chemical and phase evolution of amorphous molybdenum sulfide catalysts for electrochemical hydrogen production. *ACS Nano* **10**, 624-632 (2016).
141 Benck, J. D., Chen, Z., Kuritzky, L. Y., Forman, A. J. & Jaramillo, T. F. Amorphous molybdenum sulfide catalysts for electrochemical hydrogen production: insights into the oigin of their catalytic activity. *ACS Catal.* **2**, 1916-1923 (2012).
142 Staszak-Jirkovský, J. *et al.* Design of active and stable Co–Mo–Sx chalcogels as pH-universal catalysts for the hydrogen evolution reaction. *Nat. Mater.* **15**, 197-203 (2015).
143 Jaramillo, T. F. *et al.* Hydrogen evolution on supported incomplete cubane-type $[Mo_3S_4]^{4+}$ electrocatalysts. *J. Phys. Chem. C* **112**, 17492-17498 (2008).
144 Ji, Z., Trickett, C., Pei, X. & Yaghi, O. M. Linking molybdenum–sulfur clusters for electrocatalytic hydrogen evolution. *J. Am. Chem. Soc.* **140**, 13618-13622 (2018).
145 Kibsgaard, J., Jaramillo, T. F. & Besenbacher, F. Building an appropriate active-site motif into a hydrogen-evolution catalyst with thiomolybdate $[Mo_3S_{13}]^{2-}$ clusters. *Nat. Chem.* **6**, 248-253 (2014).
146 Huang, Z. *et al.* Dimeric $[Mo_2S_{12}]^{2-}$ cluster: A molecular analogue of $MoS_2$ edges for superior hydrogen-evolution electrocatalysis. *Angew. Chem. Int. Ed.* **54**, 15181-15185 (2015).
147 Tran, P. D. *et al.* Coordination polymer structure and revisited hydrogen evolution catalytic mechanism for amorphous molybdenum sulfide. *Nat. Mater.* **15**, 640-646 (2016).
148 Li, Y. *et al.* Engineering the composition and crystallinity of molybdenum sulfide for high-performance electrocatalytic hydrogen evolution. *ACS Catal.* **5**, 448-455 (2015).
149 Vrubel, H. & Hu, X. Growth and activation of an amorphous molybdenum sulfide hydrogen evolving catalyst. *ACS Catal.* **3**, 2002-2011 (2013).
150 Ting, L. R. L. *et al.* Catalytic activities of sulfur atoms in amorphous molybdenum sulfide for the electrochemical hydrogen evolution reaction. *ACS Catal.* **6**, 861-867 (2016).

151 T. Siegrist, P. Merkelbach & Wuttig, M. Phase change materials: challenges on the path to a universal storage device. *Annu. Rev. Condens. Matter Phys.* **3**, 215-237 (2012).
152 Deb, S. K., Wilding, M., Somayazulu, M. & McMillan, P. F. Pressure-induced amorphization and an amorphous–amorphous transition in densified porous silicon. *Nature* **414**, 528-530 (2001).
153 Zhang, X. *et al.* Lithiation-induced amorphization of $Pd_3P_2S_8$ for highly efficient hydrogen evolution. *Nat. Catal.* **1**, 460-468 (2018).
154 Wuttig, M., Bhaskaran, H. & Taubner, T. Phase-change materials for non-volatile photonic applications. *Nat. Photonics* **11**, 465-476 (2017).
155 Siegrist, T. *et al.* Disorder-induced localization in crystalline phase-change materials. *Nat. Mater.* **10**, 202-208 (2011).
156 Quan, Z. *et al.* Pressure-induced switching between amorphization and crystallization in PbTe nanoparticles. *Nano Lett.* **13**, 3729-3735 (2013).
157 Corsini, N. R. C. *et al.* Pressure-induced amorphization and a new high density amorphous metallic phase in matrix-dree Ge nanoparticles. *Nano Lett.* **15**, 7334-7340 (2015).
158 Ambrosi, A. & Pumera, M. Exfoliation of layered materials using electrochemistry. *Chem. Soc. Rev.* **47**, 7213-7224 (2018).
159 Zhang, H. Ultrathin two-dimensional nanomaterials. *ACS Nano* **9**, 9451-9469 (2015).

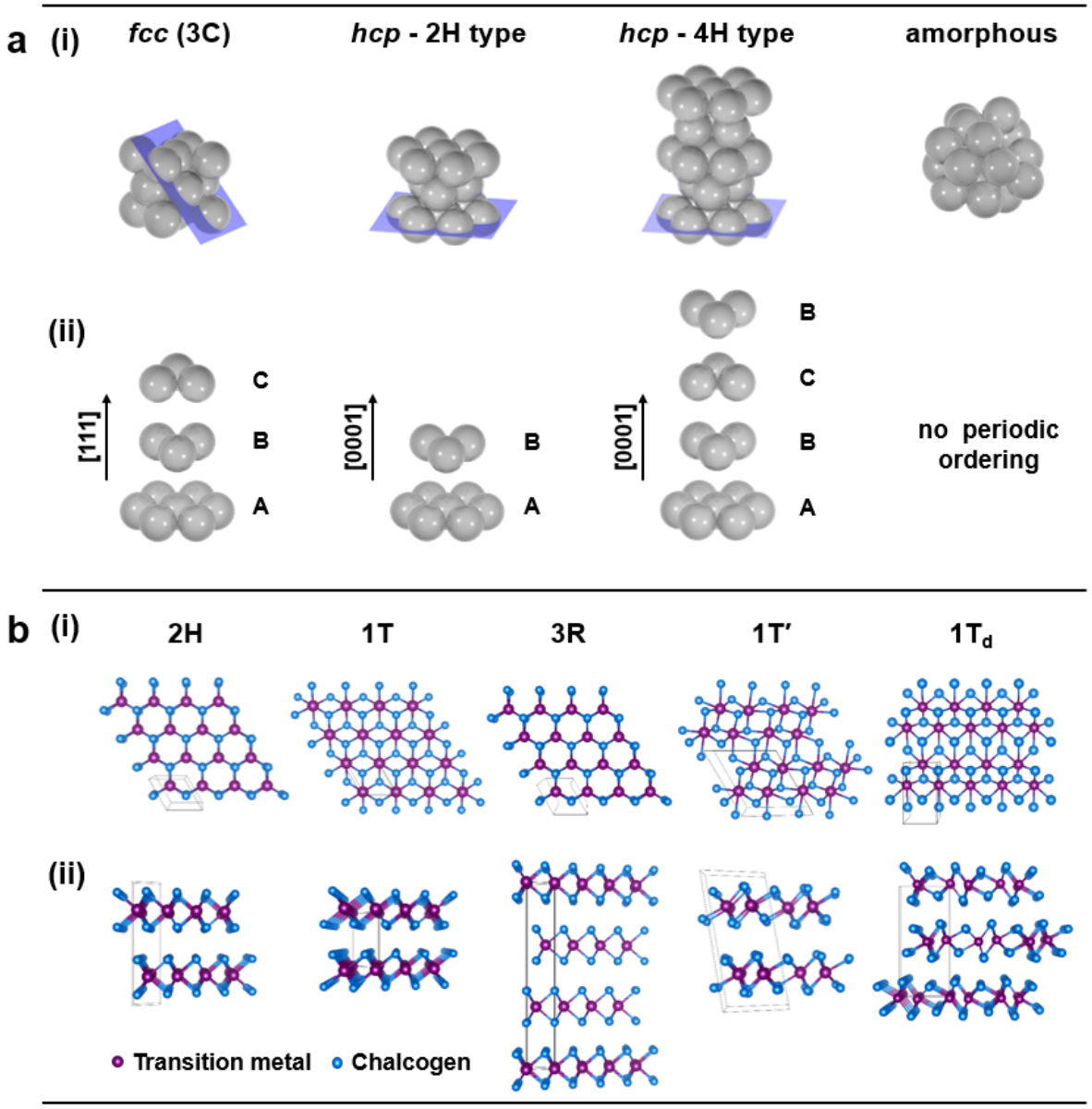


**Figure 1. Schematic models of different phases of metals and transition metal dichalcogenides. a |** Hard-ball models of face-centered cubic (*fcc*) (3C), hexagonal close-packed (*hcp*)-2H type, *hcp*-4H type crystal structures and amorphous structures. Unit cells showing the smallest repeating units of these phases, with the close-packed planes highlighted in blue (top). The characteristic packing sequences of the close-packed planes in different phases (bottom). **b |** Simulated structure models of transition metal dichalcogenides (TMDs) including hexagonal (2H), octahedral (1T), rhombohedral (3R), distorted octahedral (1T') and $1T_d$ phases. Top view showing the typical atomic arrangement of a single-layer (top). Side view showing the typical packing sequences. The unit cells of these layered structures are marked by the black lines (bottom).

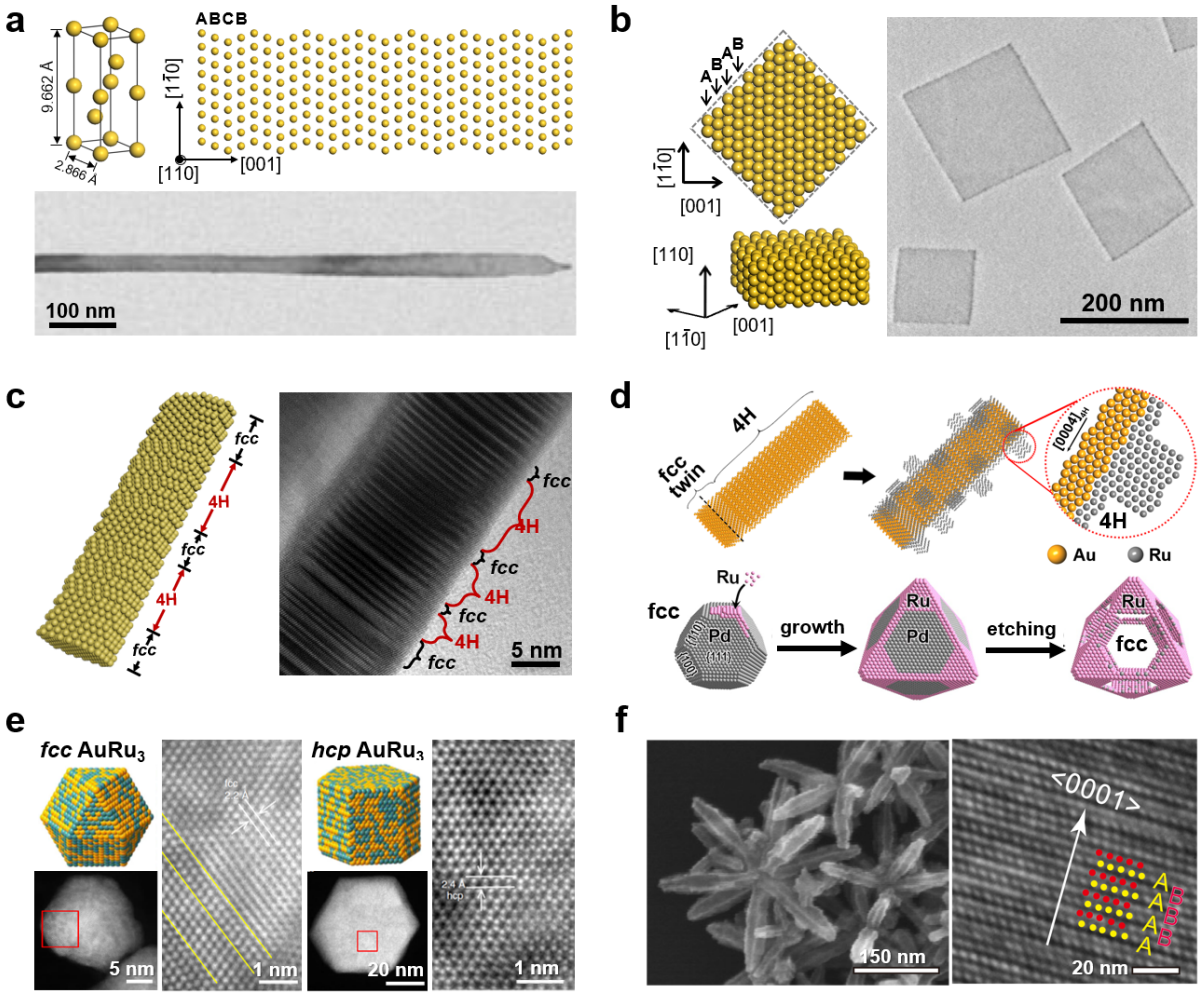


**Figure 2 | Direct synthesis of metal nanomaterials with unconventional crystal phases. a** | Au nanoribbon with the unconventional 4H-type of *hcp* phase. The simulated unit cell of 4H Au and the top view of a typical 4H Au nanoribbon (upper panel). The close-packed planes along the $[001]_{4H}$ direction show a characteristic ABCB stacking sequence. TEM image of a typical 4H Au nanoribbon (bottom panel). **b** | Au square sheets (AuSSs) with the unconventional 2H-type of *hcp* phase. Crystallographic models for a typical AuSS on a graphene oxide surface showing ABAB stacking along the $[001]_{2H}$ direction (left panel) and the typical TEM image (right panel). **c** | 4H-*fcc* crystal-phase-heterostructured Au nanorod in simulated model (left panel) and TEM image (right panel), showing 4H and *fcc* phases co-existing and randomly alternating in a single rod. **d** | Schematic illustrations of the crystal phase-based epitaxial growth of 4H-Ru on 4H-*fcc* Au nanowire (upper panel), and *fcc* Ru on *fcc* Pd nanocrystal (bottom panel). **e** | Selectively grown *fcc* and *hcp* $AuRu_3$ alloy nanoparticles by tuning the growth kinetics of Au and Ru. The left three panels show the schematic model, low magnification and high resolution TEM images of *fcc* $AuRu_3$ alloy nanoparticles, respectively. The right three panels show the schematic model, low magnification and high resolution TEM images of *hcp* $AuRu_3$ alloy nanoparticles, respectively. **f** | Low magnification scanning electron microscopy (SEM) image of the 2H excavated PtNi alloy nano-multipods (left panel) and the high resolution TEM image showing the characteristic ABAB stacking sequence (right panel). Panel **a** is adapted from REF.[29], Springer Nature Limited. Panel **b** is adapted from REF.[30], Springer Nature Limited.

Panel **c** is adapted with permission from REF.[32], Wiley-VCH. Panel **d** is adapted from REF.[40], Springer Nature Limited, and REF.[41], ACS. Panel **e** is adapted from REF.[48], Springer Nature Limited. Panel **f** is adapted from REF.[50], Springer Nature Limited.

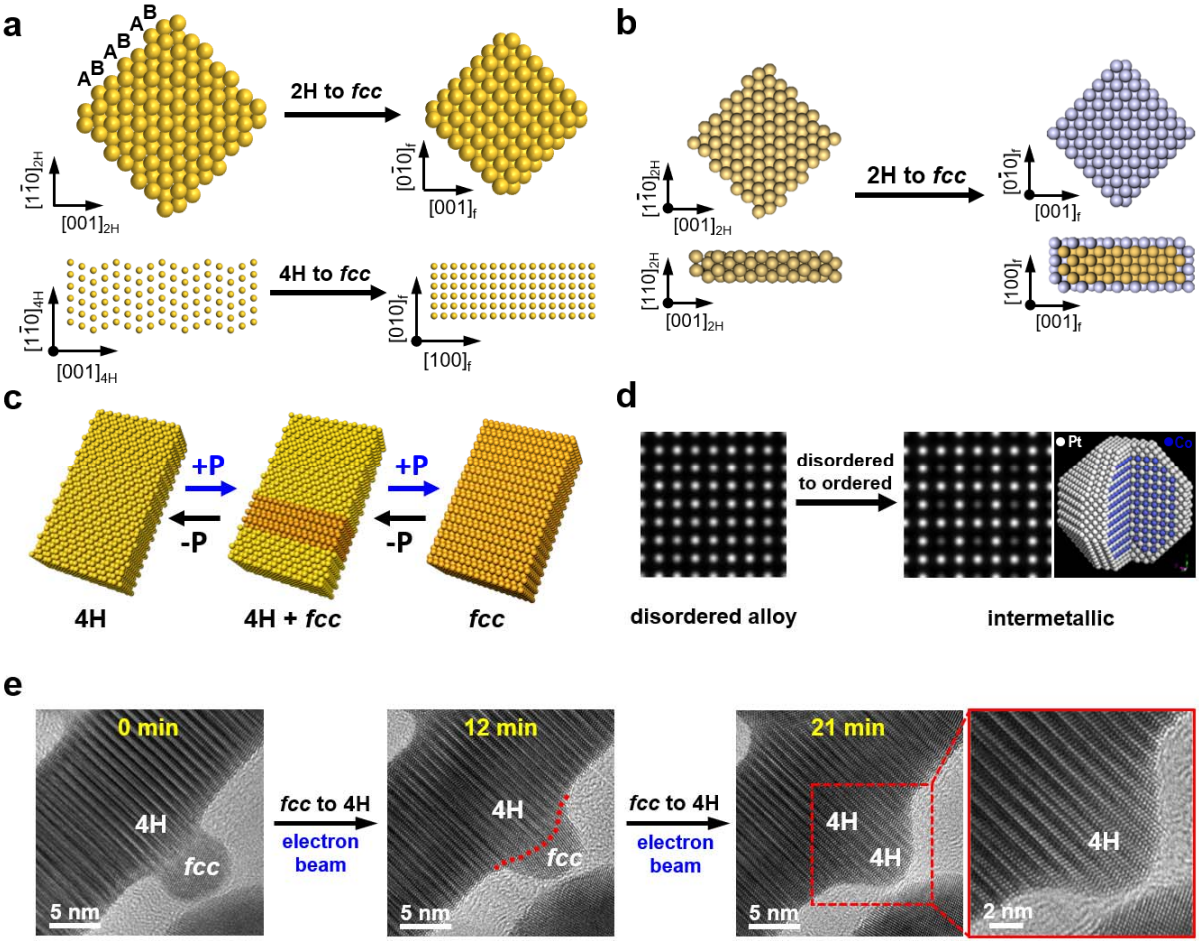


**Figure 3. Phase transformation of metal nanomaterials. a** | Schematic illustration of ligand-exchange induced phase transformation of Au square sheet (AuSS) from 2H to *fcc* phase (upper panel), and phase transformation of Au nanoribbon from 4H to *fcc* phases (bottom panel) induced by ligand exchange on the nanoparticle surface. Here, oleylamine was substituted with thiols. **b** | Schematic illustration of phase transformation of AuSS from 2H to *fcc* induced by metal-coating. **c** | High-pressure induced irreversible phase transformation of Au nanoribbons from 4H to *fcc*. **d** | Simulated annular dark field STEM (ADF-STEM) images (left panel) and atomic structure (right panel) of $Pt_3Co$ nanostructure that undergo high-temperature-induced phase transformation. High temperature aids the transition from chemically disordered Pt–Co alloy, in which all columns have equal intensity, to ordered intermetallic $Pt_3Co$ nanoparticles, in which Pt columns have higher intensity than the Co columns due to the Z-contrast in ADF-STEM image. **e** | Snapshots taken at 0, 12, 21 min of

an electron beam irradiation-induced phase transformation of a monocrystalline *fcc* Au nanoparticle adhering to the 4H nanodomain of a 4H/*fcc* Au nanorod during the *in situ* TEM imaging. The 4H-*fcc* phase boundary is indicated in red. Panels **a** is adapted from REF.[52] and REF.[29], Springer Nature Limited. Panel **b** is adapted from REF.[52], Springer Nature Limited. Panel **c** is adapted with permission from REF.[53], ACS. Panel **d** is adapted from REF.[54], Springer Nature Limited. Panel **e** is adapted from REF.[70], Wiley-VCH.

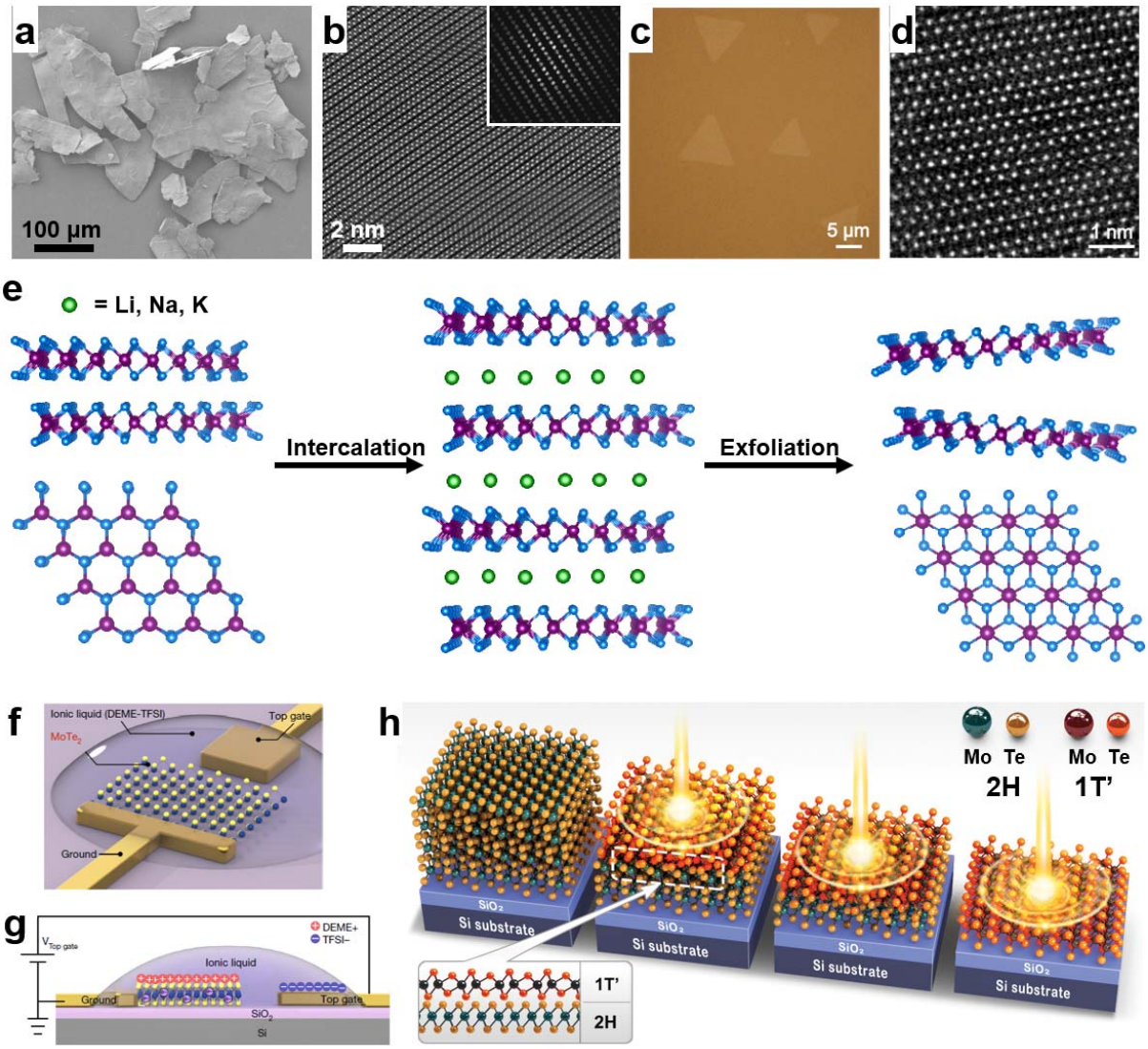


**Figure 4. Direct synthesis and phase transformation of transition metal dichalcogenides (TMDs). a |** Scanning electron microscopy image (SEM) of 1T'-$MoS_2$ crystals obtained by gas–solid reaction. **b |** Scanning transmission electron microscopy (STEM) image of a single-layer 1T'-$MoS_2$ nanosheet exfoliated from the 1T'-$MoS_2$ crystal, showing the characteristic zigzag atomic arrangement.**c |** Optical image of monolayer 1T'-$MoS_2$ grown by chemical vapour deposition (CVD) method. **d |** Atomically resolved filtered STEM images of a monolayer of 1T'-$MoS_2$ grown ona mica substrate, showing the characteristic zig-zag atomic arrangement. **e |** Schematic illustration of alkali metal ion-assisted exfoliation, which could simultaneously induce the phase transformation of TMDs. **f |** Schematic illustration of a

monolayer $MoTe_2$ top-gate field effect transistor (FET) in the ionic liquid (N,N-diethyl-N-(2-methoxyethyl)-N-methylammonium bis(trifluoromethylsulphonyl-imide), DEME–TFSI). **g** |Measurement configuration of the single-layer $MoTe_2$ FET with $DEME^+$ layer on the cathode ($MoTe_2$) and $TFSI^-$ layer on the anode. Ionic gating strongly manipulated the electron population in the single-layer $MoTe_2$, resulting in a phase transition from 2H to 1T' phases. **h** | Schematic illustration of the laser-induced phase transition of multi-layer $MoTe_2$ from 2H to 1T'. A thinning effect was observed and the phase transition only occurred at the top layer of the multi-layer $MoTe_2$. Panels **a** and **b** are adapted from REF.[76], Springer Nature Limited. Panels **c** and **d** are adapted from REF.[78], Springer Nature Limited. Panels **f** and **g** are adapted from REF.[85], Springer Nature Limited. Panel **h** is adapted from REF.[83], AAAS.

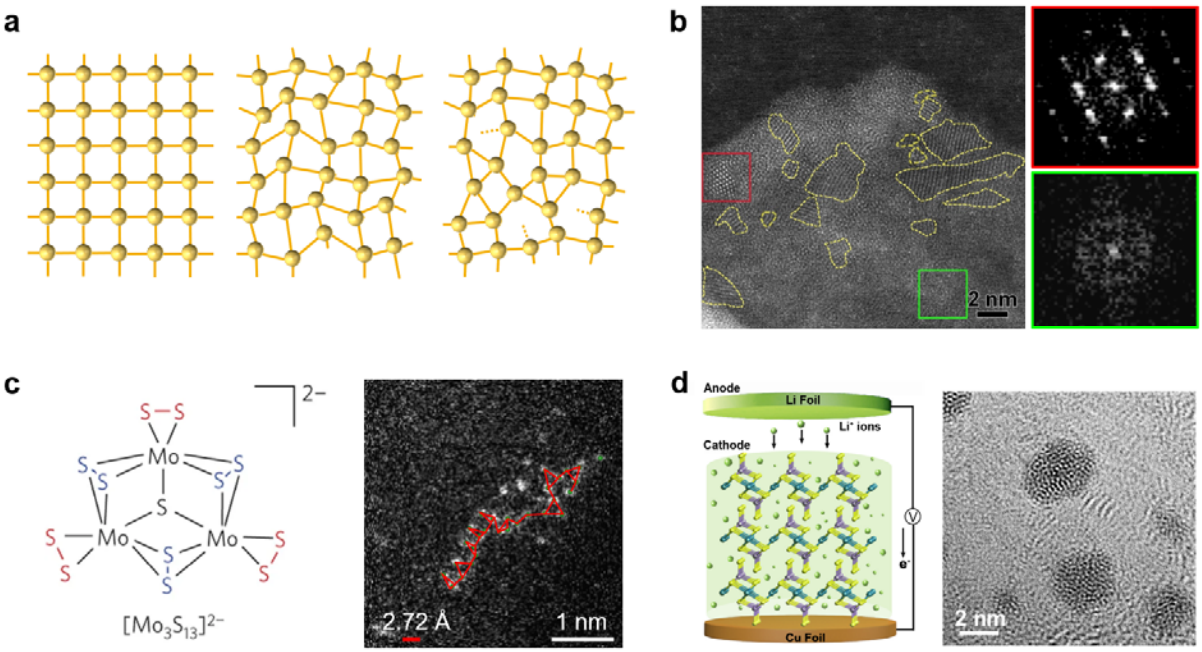


**Figure 5. Amorphous and amorphous/crystalline nanomaterials. a** | Schematic illustrations of an ideal crystal (left panel), amorphous structure with distorted lattice (centre panel), and amorphous structure with distorted lattice and dangling bonds (right panel). The dotted lines represent the dangling bonds. **b** | STEM image of an amorphous/crystalline heterophase Pd nanosheet (left panel) and the fast Fourier transform patterns of crystalline and amorphous regions (right panel), where the bright spots (red square) and the diffuse ring (green square) are used to identify the crystalline and amorphous domains, respectively. The crystalline regions are marked in dashed yellow curves (left panel). **c** | The atomic structure (**left panel**) and TEM image (**right panel**) of amorphous $MoS_x$, showing the arrangement of $[Mo_3]$ cluster units in a one-dimensional unfolding chain shown in red. **d** | Schematic illustration of the preparation of amorphous ultrasmall Li-incorporated palladium

phosphosulfide nanodots from layered bulk $Pd_3P_2S_8$ crystals using the electrochemical lithiation method (**left panel**) and the high resolution TEM image of the as-obtained amorphous nanodots (**right panel**). The lithiation-induced amorphization of the $Pd_3P_2S_8$ crystal was carried out by conducting galvanostatic discharge in a columnar Li-ion battery cell with fragments of $Pd_3P_2S_8$ flake as the cathode and Li foil as the anode. Panel **b** is adapted with permission from REF.[130], Wiley-VCH. Panels **c** and **d** are adapted from REF.[147], Springer Nature Limited. Panels **e** and **f** are adapted from REF.[153], Springer Nature Limited.